ACS APPLIED MATERIALS & INTERFACES

Research Article

Cite This: ACS Appl. Mater. Interfaces 2019, 11, 36800−36806

www.acsami.org

Strain-Inhibited Electromigration of Oxygen Vacancies in $LaCoO_3$

Liang Zhu,[†,§] Shulin Chen,[‡,⊥] Hui Zhang,[†,§] Jine Zhang,[†,§] Yuanwei Sun,[‡] Xiaomin Li,[‡] Zhi Xu,[†,∥] Lifen Wang,[*,†] Jirong Sun,[†,§,∥] Peng Gao,[‡,#] Wenlong Wang,[*,†,∥] and Xuedong Bai[*,†,§,∥]

[†]Beijing National Laboratory for Condensed Matter Physics, Institute of Physics, Chinese Academy of Sciences, Beijing 100190, China

[‡]Electron Microscopy Laboratory, and International Center for Quantum Materials, School of Physics, Peking University, Beijing 100871, China

[§]School of Physical Sciences, University of Chinese Academy of Sciences, Beijing 100190, China

[∥]Songshan Lake Materials Laboratory, Dongguan, Guangdong 523808, China

[⊥]State Key Laboratory of Advanced Welding and Joining, Harbin Institute of Technology, Harbin 150001, China

[#]Collaborative Innovation Center of Quantum Matter, Beijing 100871, China

Supporting Information

ABSTRACT: The oxygen vacancy profile in $LaCoO_3$ exhibits rich phases with distinct structures, symmetries, and magnetic properties. Exploration of the lattice degree of freedom of $LaCoO_3$ in the transition between these different structural phases may provide a route to enable new functionality in oxide materials with potential applications. To date, the oxygen vacancy profile transition in $LaCoO_3$ has mainly been induced by transition-metal doping or thermal treatment. Epitaxial strain was proposed to compete with the lattice degree of freedom but has not yet been rationalized. Here, the experimental findings of strain-inhibited structural transition from perovskite to brownmillerite during the electromigration of oxygen vacancies in epitaxial $LaCoO_3$ thin films are demonstrated. The results indicate that the oxygen vacancy ordering phase induced by the electric field is suppressed locally by both epitaxial strain field and external loads shown by *in situ* aberration-corrected (scanning)/ transmission electron microscopy. The demonstrated complex interplay between the electric and strain fields in the structural transitions of $LaCoO_3$ opens up prospects for manipulating new physical properties by external excitations and/or strain engineering of a substrate.

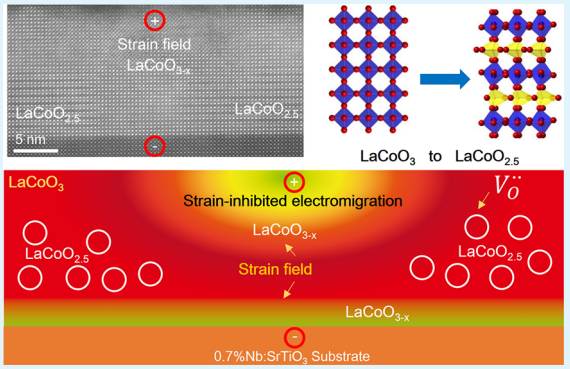

KEYWORDS: *oxygen vacancy migration, perovskite, phase transition, strain field, in situ TEM*

INTRODUCTION

Transition metal oxides with a perovskite structure (ABO_3) are relevant to a vast array of functional applications such as solid oxide fuel cells,[1] resistive random access memory,[2] spintronic devices,[3−5] gas sensors,[6−8] and oxygen permeation membranes[9] due to their high oxygen-ionic conductivity.[10] As one of the most important features for determining the physical properties of transition metal oxides, oxygen vacancies with distinct structural phases formed in nonstoichiometric perovskites play the key role[11] and can be effectively employed to tune the functionality of transition metal oxides ranging from superconductivity,[12] ferromagnetism,[3,4,13,14] and metal-to-insulator transition[15−17] to interface conductivity.[18,19] For instance, epitaxial $LaCoO_3$ films with multiple oxygen vacancy orderings corresponding to rich structural phases have demonstrated a range of applications.[20−22] Even though the nature of the structural phase transition in epitaxial $LaCoO_3$ film remains unclear, the diverse phases in epitaxial $LaCoO_3$ thin films are recognized to be closely related to the oxygen vacancy ordering.[20,21,23] To manipulate the phase with controlled properties, strain has been demonstrated to be a crucial parameter for enhancing or suppressing the diverse properties of transition metal oxides and may also break the balance of the competing degrees of freedom of the lattice, symmetry, electron, etc.[23−27] Therefore, correlating the strain field with the dynamic oxygen vacancy ordering phase in perovskite oxides is of vital importance to both fundamental study and applications; however, the relationship between the strain and the oxygen vacancy ordering phase which is crucial for understanding the physical properties of oxide materials has been hardly reported.

In this study, utilizing *in situ* transmission electron microscopy (TEM), the dynamic processes of oxygen vacancy electroformation and migration in epitaxial $LaCoO_3$ thin film

Received: May 14, 2019
Accepted: September 20, 2019
Published: September 20, 2019

DOI: 10.1021/acsami.9b08406
ACS Appl. Mater. Interfaces 2019, 11, 36800−36806

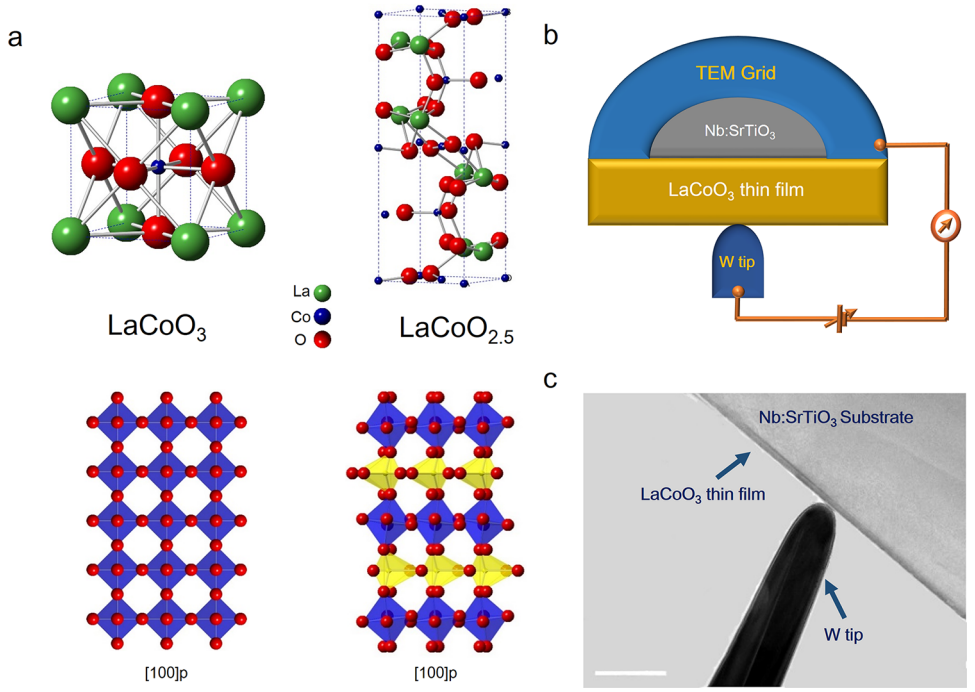

Figure 1. Configuration of the experimental setup. a Crystal structures of $LaCoO_3$ and $LaCoO_{2.5}$ along the pseudocubic [100] direction. b Schematic of *in situ* TEM experimental setup. c TEM image of the W tip/$LaCoO_3$/NSTO structure. Scale bar is 200 nm.

with or without an external load applied were observed. Our results show that the strain from both epitaxial and external loads can inhibit the oxygen vacancy electromigration and thus control the position and orientation of the oxygen vacancy ordering phase. The demonstrated ability to simultaneously drive the oxygen vacancy migration and manipulate the oxygen vacancy ordering in $LaCoO_3$ will open prospects for mesoscale quantum phenomena and tailoring physical properties of functional oxides.

RESULTS AND DISCUSSION

In situ TEM with improved resolution and contrast provides an ideal method to characterize the dynamic behavior of oxygen vacancies in perovskites.[28−30] Figure 1a shows a schematic of the crystal structure of the perovskite $LaCoO_3$ and brownmillerite $LaCoO_{2.5}$. Through a strong interaction between the lattice and electronic degrees of freedom, the phase transition from $LaCoO_3$ to $LaCoO_{2.5}$ can be achieved by converting the stacks of $[CoO_6]$ octahedral layers to alternating stacks of $[CoO_4]$ tetrahedral and $[CoO_6]$ octahedral layers.[22] To study the dynamic process of the phase transition through oxygen migration, a sandwiched junction of W tips (deep blue), $LaCoO_3$ thin film (golden) grown epitaxially on a (001) 0.7%Nb-doped $SrTiO_3$(NSTO) conductive substrate (gray) and a Mo grid as the current collector was constructed inside the TEM, as shown in Figure 1b and c. The sharp tungsten (W) tip driven by a piezo controller plays a double-acting role in the *in situ* experiment. First, it is used as a movable electrode that achieves electrical contact with the $LaCoO_3$ thin film. Second, it is used as a mechanical tip to provide an external load. The samples, which were approximately 20 nm thick $LaCoO_3$ films grown epitaxially on NSTO by pulsed laser deposition (see Supporting Information (SI) Figures S1 and S2), were thinned to electron transparency by traditional mechanical polishing and argon ion milling. Due to the lattice mismatch between the NSTO and $LaCoO_3$ thin film, a 2.6% tensile strain is imposed upon the interface. Electrical contacts to the NSTO side were made by attaching it to a half Mo grid (blue) using silver paste.

The perovskite $LaCoO_3$ to brownmillerite $LaCoO_{2.5}$ transition occurring simultaneously upon the application of an anodizing electric filed was recorded by *in situ* TEM. Figure 2 depicts the dynamic process of oxygen vacancy migration in epitaxial $LaCoO_3$ thin film upon applying a bias of 2 V (W tips as the anode) and a proper strain to the epitaxial $LaCoO_3$ thin film by a piezo controller. The gray area in the sample indicates amorphous depletion from mechanical preparation. After both the electric (+2 V) and strain fields (the distance between the

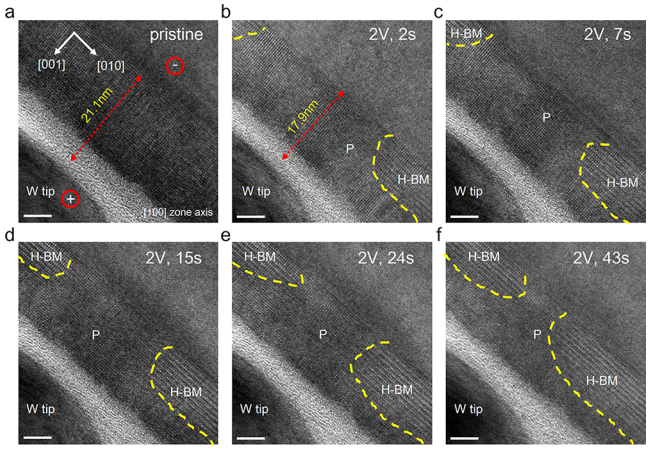

Figure 2. HRTEM images along the [100] zone axis depicting the dynamic process of oxygen vacancy migration under both electric and strain fields. a. Pristine $LaCoO_3$ thin film. b−f. A series of high-resolution TEM images illustrating the growth of the H-BM phases. Red arrow indicates the distance between the W tip and $SrTiO_3$ substrate. Yellow dashed lines in the TEM images indicate the boundary between the H-BM and P phases. Scale bars are 5 nm.

DOI: 10.1021/acsami.9b08406
ACS Appl. Mater. Interfaces 2019, 11, 36800−36806

W tip and the NSTO substrate reduced from 21.1 to 17.9 nm) were applied across the pristine $LaCoO_3$ film (P phase) for 2 s, a horizontal brownmillerite phase (H-BM phase, $LaCoO_{2.5}$) due to the oxygen moving out from every other CoO_x layer appeared first on both sides of the W tips near the NSTO substrate as visualized in Figure 2b. Subsequently, the H-BM phases started to grow from the edge to the center as shown sequentially in Figure 2c–f. In this transition progress, the $LaCoO_3$ retained its pristine structure in front of the tip area (see SI Video M1, SI Figure S3) where the external load was applied. Energy dispersive X-ray spectroscopy (EDS) also confirms a significant decrease in the oxygen content in the area showing oxygen vacancy ordering phase (see SI Figure S4). When the strain was applied to the $LaCoO_3$, the oxygen migration induced by the external electric field tends to be parallel to the $LaCoO_3/SrTiO_3$ interface along the [010] direction, and oxygen migration along the [001] direction, which is perpendicular to the $LaCoO_3/SrTiO_3$ interface, was hardly ever observed. Due to the strain-inhibited electromigration along the [001] direction, the oxygen migration is apparently anisotropic. Thus, the direction of the propagation of the modulation wave, which was in accord with the horizontal component of the electric field, was preferentially parallel to the interface. Nevertheless, the vertical modulation wave could be sometimes observed in a much flatter tip with a smaller force that is not sufficient to completely inhibit oxygen migration in front of the W tip (see SI Figure S5 and Video M2). Based on real-time structural characterization, the electric and strain fields demonstrate a strong interplay in the oxygen vacancy ordering phase formation in $LaCoO_3$ such that the oxygen vacancy profile follows the electric flux line, while it is pinned by strain field. Thus, the most likely scenario for the structural transition in $LaCoO_3$ is that oxygen is being driven out by the electric field while the strain field pins the structure with the pristine phase demonstrating strain-inhibited electromigration of oxygen vacancies.

To understand the driving force of the structural transition, in comparison with the dynamic process under both electric and strain fields, the oxygen migration process in which the W tips act only as electric contacts (not applying mechanical force) with the $LaCoO_3$ thin film was recorded in Figure 3a–c. By contrast, in absence of the inhibition of the strain field from the W tips, the H-BM phase appeared first in the surface of the thin film near the W tip and grew laterally due to the lateral component of electric field. Simultaneously, the vertical brownmillerite phase (V-BM phase, $LaCoO_{2.5}$) appeared in the surface of the thin film right in front of the SPM tip and grew from the surface to the interface gradually, as shown in Figure 3b and c (see also SI Videos M3 and M4 and Figure S6). The electric field distribution in the $LaCoO_3$ thin film on which the direction of the oxygen vacancy ordering phase depends is depicted in Figure 3d. Similarly, to eliminate the possibility that the oxygen vacancy ordering is induced by strain alone, the experiment that only proper strain field was applied to the $LaCoO_3$ thin film was conducted. With the film loaded, no obvious superstructure or extra diffraction pattern appeared, indicating that the mechanical strain field hardly contributes to the generation of the new oxygen vacancy ordering phase, as shown in Figure 3e,f (see SI Video M5).

External loads have revealed the strong pinning effect on the oxygen vacancy ordering phase formation based on the above experiments. Epitaxial strain effect was also confirmed by the *in situ* aberration-corrected STEM here as shown in Figure 4. To

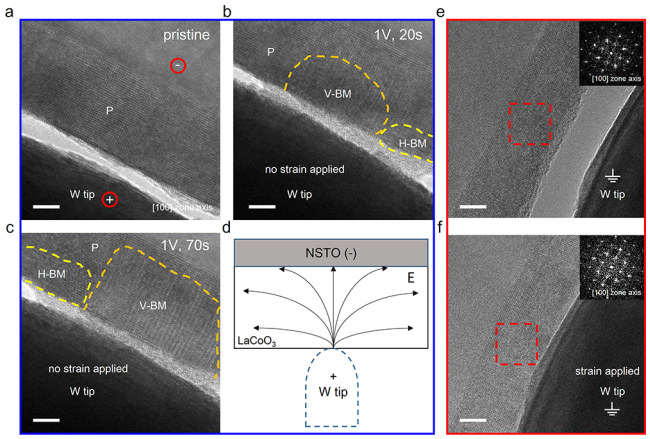

Figure 3. Oxygen vacancy migration in $LaCoO_3$ thin film under electric or strain field only. a. HRTEM image of a pristine $LaCoO_3$ thin film along the [100] direction. b, c. Structure evolution during the application of an electric field. d. Electric field distribution in the LaCoO3 thin film. e, f. HRTEM images of $LaCoO_3$ without and with strain field applied from an SPM tip and the corresponding FFT patterns from the red rectangle. The yellow dashed lines in the TEM images indicate the boundary between the H-BM and P phases. The orange dashed lines indicate the boundary between the vertical brownmillerite (V-BM, $LaCoO_{2.5}$) and P phases. Scale bars are 5 nm.

probe the distribution of oxygen ions or vacancies in the thin film before and after the phase transition by applying both electric and strain fields from the W tip, high angle annular dark-field (HAADF) scanning transmission electron microscopy (STEM) images were obtained along the pseudocubic [100] direction. In this imaging mode, the intensity of the atomic column is approximately proportional to Z^2, where Z is the atomic number.[31] Thus, La atoms with higher atomic number Z appear brighter and Co atoms appear fainter. Atomic columns containing oxygen contribute negligibly to the image intensity. The STEM HAADF images of pristine $LaCoO_3$ and the film imposed by both electric and strain fields from the W tip are shown in Figure 4a and b, respectively. The pristine $LaCoO_3$ thin film exhibits a uniform contrast, showing even thickness and stoichiometry. The modulation of the HAADF intensity (marked as area B) was measured in every second CoO_x plane of the superstructure after the oxygen vacancies were introduced by external fields as shown in Figure 4b. The superstructure features oxygen vacancy ordering.[21] The oxygen was depleted from every other CoO_x layer along the *c*-direction, causing vertical displacement of the La atoms. However, no obvious superstructures in the interface (marked as area C) and the top region (marked as area A) are observed, implying an evident inhibition of electromigration by the strain field from the epitaxial NSTO substrate and the mechanical load provided by the mechanical tip. To zoom in the distinct phase transition before and after the application of external fields, Figure 4c and d show enlarged high-resolution STEM images of the area marked by the yellow rectangles in Figure 4a and b, respectively. Maps of the out of plane lattice spacing between La–La ions in Figure 4c and d are shown in Figure 4e and f, respectively. Depletion of oxygen reduces the coordination of Co cations, causing an elongation of the out of plane lattice spacing by the chemical expansion. A clear modulation of the La–La lattice spacing is presented in Figure 4f. By contrast, the interface area and the top region near the tip have a smaller lattice spacing, implying

DOI: 10.1021/acsami.9b08406
ACS Appl. Mater. Interfaces 2019, 11, 36800–36806

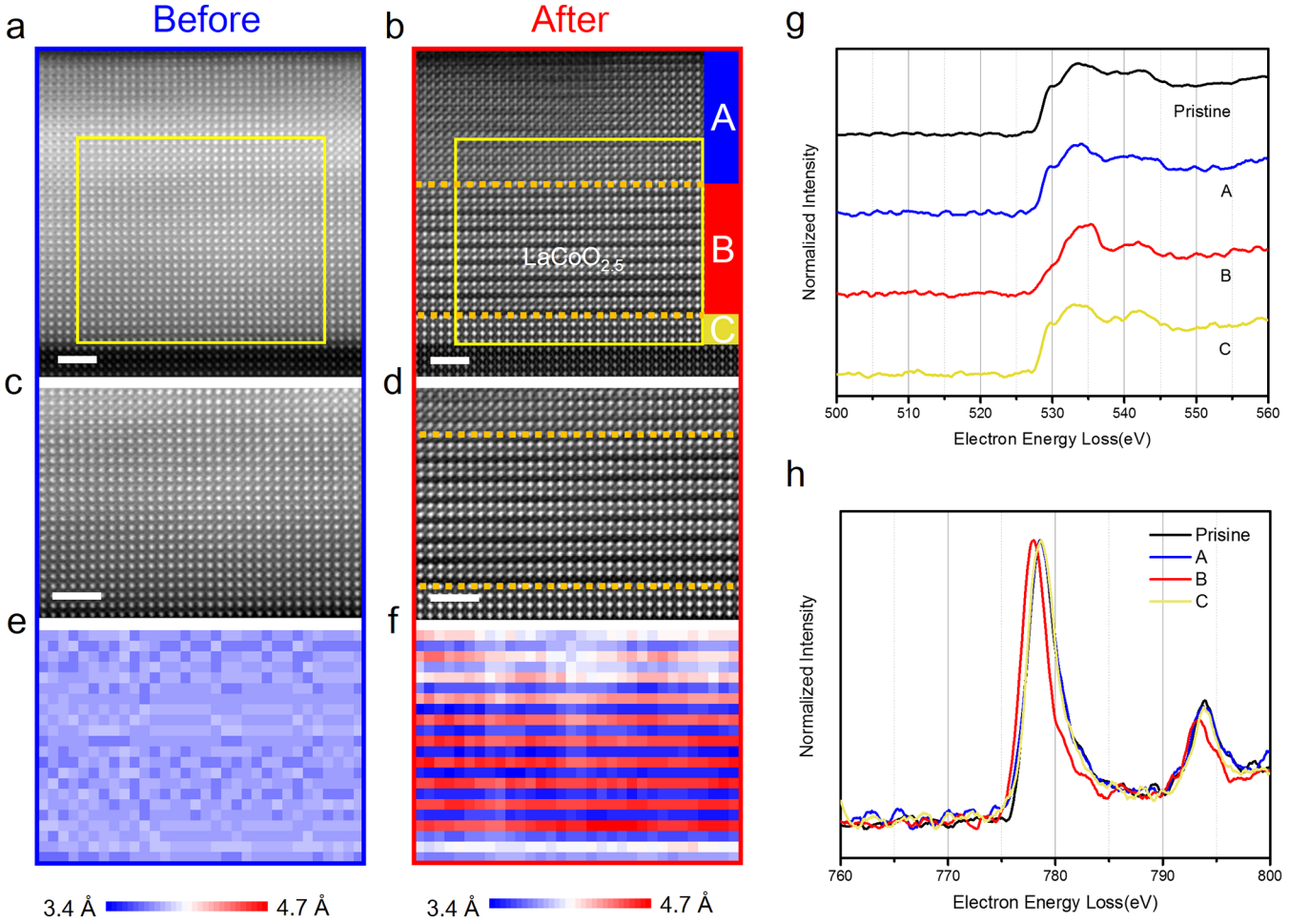

Figure 4. Changes in the atomic and electronic structure during the phase transition. a,b. STEM HAADF images along the [100] zone axis of the $LaCoO_3$ thin film before and after electric and strain fields were applied, respectively. c, d. Enlarged STEM HAADF images of the yellow rectangles in (a) and (b), respectively. e, f. Maps of the out of plane La−La lattice spacing in (c) and (d), respectively. g, h STEM-EELS of the O−K edges and the Co-$L_{2,3}$ edges for the pristine $LaCoO_3$ and the three regions marked as A, B, and C in (b). Scale bars are 2 nm.

the presence of strain-inhibited electromigration of oxygen vacancies in epitaxial $LaCoO_3$ thin film.[32]

In addition to the changes in the atomic structure, the electronic structure is also dramatically altered. The hindered oxygen vacancy migration under both electric and strain fields was further confirmed by electron energy loss spectroscopy (EELS). The EELS of the O−K edges and Co-$L_{2,3}$ edges from the pristine $LaCoO_3$ and the three regions marked as A, B, and C in Figure 4b are shown in Figure 4g and h, respectively. Focusing on the O−K edge in Figure 4g, three main features can be confirmed for the $LaCoO_3$ thin film. A prepeak at approximately 530 eV is related to the filling of the hybridized O 2p and Co 3d states.[33,34] The peak at approximately 535 eV (the first main peak) is commonly attributed to the La 5d band, whereas the peak at approximately 540 eV (the adjacent peak) derives from the Co 4sp band.[33] The prepeak of O−K edge related to the filling of hybridized O 2p and Co 3d states of region B decreased when compared with those in region A and C, indicating many more oxygen vacancies were created and the valence of Co decreased.[35] Region A and C have almost the same concentration of oxygen vacancies as the pristine $LaCoO_3$. Figure 4h demonstrates the Co-$L_{2,3}$ edge contrast. The increase in the Co L_3/L_2 ratio in region B compared with those in region A and C implies a decrease in the Co oxidation state as well.[36]

By taking advantage of the state of the art *in situ* TEM and aberration-corrected STEM, we have revealed the unique dynamic $LaCoO_3$ to $LaCoO_{2.5}$ phase transition under both electric and strain fields. The oxygen ions were extracted from every other CoO_x layer. Oxygen vacancy migration driven by an external electric field is hindered by the applied strain field. Thus, the strain field can be used as an effective approach to tune the oxygen vacancy ordering phase. Different orientations of oxygen vacancy ordering through the strain-tuned oxygen migration in the $LaCoO_3$ were achieved in this work.

The underlying mechanism of the strain-inhibited oxygen vacancy migration process is illustrated in Figure 5 based on the above-described results. The strain field distribution after the W tip touched the film is shown schematically in Figure 5a. Due to the inhibition of oxygen migration by the strain field, the oxygen vacancies driven by the electric field tend to be generated at both sides of the thin film transforming the material from the pristine P phase to the H-BM phase. The oxygen migration in the [001] direction was effectively inhibited by the strain field while it is anisotropic in the [010] and [001] directions. In this process, the strain field can be regarded as an effective parameter to inhibit the chemical expansion caused by oxygen migration, thus inhibiting the phase transition. By contrary, in the absence of an application of strain to the thin film, the oxygen vacancies driven by

DOI: 10.1021/acsami.9b08406
ACS Appl. Mater. Interfaces 2019, 11, 36800−36806

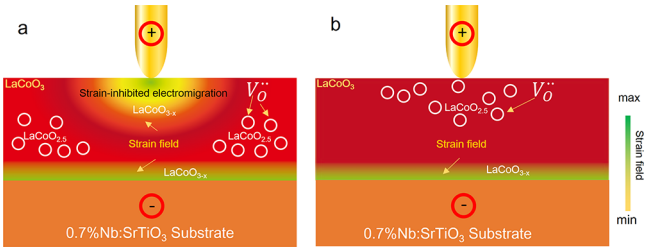

Figure 5. Underlying mechanism of the phase transition tuned by external fields. a. Schematic of the strain field distribution (induced by SPM tips and NSTO substrate) and oxygen vacancies in $LaCoO_3$ thin film after both electric and strain fields were applied through an SPM tip. b. Schematic of the strain field distribution (induced by the NSTO substrate only) and oxygen vacancies in $LaCoO_3$ thin film after electric field only was applied through an SPM tip.

electric field tend to be generated in the surface of the $LaCoO_3$ thin film to transform the material mainly from the pristine P structure to the V-BM phase or a few H-BM phases in the surface, as shown in Figure 5b.

CONCLUSIONS

In summary, our studies rationalized the strain-tuned oxygen profiles in epitaxial $LaCoO_3$ thin film and demonstrated the controllable oxygen vacancy ordering phase generation. Our method for tuning the oxygen vacancy profile provides a versatile platform for studying the fundamental physics of the lattice degrees of freedom in oxide materials. The newly revealed dynamic mechanism of oxygen vacancy ordering in the perovskite $LaCoO_3$ to brownmillerite $LaCoO_{2.5}$ transition tuned by the strong interplay of electric and strain field opens a new approach to manipulate the physical properties in functional oxides.

METHODS

Film growth. Epitaxial $LaCoO_3$ films were grown on a conducting single crystal $SrTiO_3$ (100) substrate (0.7%Nb: doped $SrTiO_3$, NSTO) by pulsed laser deposition. The growth of the films was carried out at a substrate temperature of 973 K, oxygen pressure of 20 Pa, pulse repetition rate of 2 Hz and laser fluence of 2.5 J/cm^{-2}. The film thickness is 20 nm, as determined by deposition time. After deposition, the films were cooled down under 200 Pa oxygen.

***In situ* TEM Sample Preparation.** TEM cross-sectional samples were prepared by conventional mechanical polishing and argon ion milling to electron transparency with a thickness of approximately 30−70 nm at the center region of the samples, as was estimated by the ratio between the plasmon loss and zero loss peaks in EELS spectra.

***In situ* TEM Measurements.** *In situ* measurements were conducted in a JEOL 2010F TEM instrument combined with an Agilent B2900 precision Source/Measure Unit (SMU) at an accelerating voltage of 200 kV. The TEM holders in our experiments were dedicatedly made for in situ TEM experiments by PicoFemto. The W tips, driven by a nanomanipulator as a movable top electrode for in situ measurements, were made using a homemade electrochemical corrosion cell using 5 mol/L KOH solution electrolyte. The tips were typically 30 nm at the sharpest end.

STEM Characterization. Atomically resolved STEM images were acquired using an aberration-corrected FEI Titan Themis G2 microscope operated at an accelerating voltage of 300 kV with a beam current of 120 pA, a convergence semiangle of 25 mrad, and a collection semiangle snap in the range of 53−260 mrad.

ASSOCIATED CONTENT

Supporting Information

The Supporting Information is available free of charge on the ACS Publications website at DOI: 10.1021/acsami.9b08406.

Video M1: Dynamic process of oxygen vacancy migration under both electric and strain fields (AVI)

Video M2: Dynamic process of oxygen vacancy migration under electric field with a smaller strain field (AVI)

Addition details and figures on the XRD and cross-section TEM images of epitaxial $LaCoO_3$ thin film, STEM-HAADF image of the film with both electric and strain field applied, EDS of the film before and after both electric and strain fields were applied, a series of images of oxygen vacancy migration with or without a smaller strain field from the W tip (PDF)

Videos M3 and M4: Dynamic process of oxygen vacancy migration under electric field without the strain field (AVI)

Video M4: (AVI)

Video M5: Dynamic process of oxygen vacancy migration with only the strain field applied (AVI)

AUTHOR INFORMATION

Corresponding Authors

*(L.W.) E-mail: wanglf@iphy.ac.cn.
*(W.W.) E-mail: wwl@iphy.ac.cn.
*(X.B.) E-mail: xdbai@iphy.ac.cn.

ORCID

Liang Zhu: 0000-0001-7220-7965
Jine Zhang: 0000-0001-7949-3239
Lifen Wang: 0000-0002-8468-5048
Jirong Sun: 0000-0003-1238-8770
Peng Gao: 0000-0003-0860-5525
Xuedong Bai: 0000-0002-1403-491X

Author Contributions

X.B. and W.W. conceived the idea and directed the project. L.Z. performed *in situ* TEM experiments. L.Z. and L.W. analyzed the data and wrote the paper. J.Z. grew $LaCoO_3$ films under the guidance of J.S.; Z.X. and X.L. provided technical support for *in situ* TEM holders. S.C. and Y.S. performed structural analysis under the guidance of P.G.; all of the authors discussed the results and commented on the manuscript.

Notes

The authors declare no competing financial interest.

ACKNOWLEDGMENTS

This work was supported by the Program from Chinese Academy of Sciences (ZDYZ2015-1, XDB30000000, XDB07030100, and Y8K5261B11), National Natural Science Foundation (11974388, 21872172, 51472267, 51672007, 221322304, 11290161, 51572233, 61574121, 21773303, and 51421002), National Key R&D Program (2016YFA0300804, 2016YFA0300903), the National Program for Thousand Young Talents of China, and "2011 Program" Peking-Tsinghua-IOP Collaborative Innovation Center of Quantum Matter.

DOI: 10.1021/acsami.9b08406
ACS Appl. Mater. Interfaces 2019, 11, 36800−36806

REFERENCES

(1) Shao, Z. P.; Haile, S. M. A High-Performance Cathode for the Next Generation of Solid-Oxide Fuel Cells. *Nature* **2004**, *431*, 170−173.

(2) Waser, R.; Aono, M. Nanoionics-Based Resistive Switching Memories. *Nat. Mater.* **2007**, *6*, 833−840.

(3) Cui, B.; Song, C.; Li, F.; Zhong, X. Y.; Wang, Z. C.; Werner, P.; Gu, Y. D.; Wu, H. Q.; Saleem, M. S.; Parkin, S. S. P.; Pan, F. Electric-field Control of Oxygen Vacancies and Magnetic Phase Transition in a Cobaltite/Manganite Bilayer. *Phys. Rev. Appl.* **2017**, *8*, 044007. DOI: 10.1103/PhysRevApplied.8.044007

(4) Li, H.-B.; Lu, N.; Zhang, Q.; Wang, Y.; Feng, D.; Chen, T.; Yang, S.; Duan, Z.; Li, Z.; Shi, Y.; Wang, W.; Wang, W.-H.; Jin, K.; Liu, H.; Ma, J.; Gu, L.; Nan, C.; Yu, P. Electric-field Control of Ferromagnetism through Oxygen Ion Gating. *Nat. Commun.* **2017**, *8*, 2156. DOI: 10.1038/s41467-017-02359-6

(5) Lu, N.; Zhang, P.; Zhang, Q.; Qiao, R.; He, Q.; Li, H.-B.; Wang, Y.; Guo, J.; Zhang, D.; Duan, Z.; Li, Z.; Wang, M.; Yang, S.; Yan, M.; Arenholz, E.; Zhou, S.; Yang, W.; Gu, L.; Nan, C.-W.; Wu, J.; Tokura, Y.; Yu, P. Electric-Field Control of Tri-State Phase Transformation with a Selective Dual-Ion Switch. *Nature* **2017**, *546*, 124−128.

(6) Fergus, J. W. Perovskite Oxides for Semiconductor-Based Gas Sensors. *Sens. Actuators, B* **2007**, *123*, 1169−1179.

(7) Obayashi, H.; Sakurai, Y.; Gejo, T. Perovskite-Type Oxides as Ethanol Sensors. *J. Solid State Chem.* **1976**, *17*, 299−303.

(8) Toan, N. N.; Saukko, S.; Lantto, V. Gas Sensing with Semiconducting Perovskite Oxide $LaFeO_3$. *Phys. B* **2003**, *327*, 279−282.

(9) Teraoka, Y.; Zhang, H. M.; Furukawa, S.; Yamazoe, N. Oxygen Permeation through Perovskite-Type Oxides. *Chem. Lett.* **1985**, *14*, 1743−1746.

(10) Hayashi, H.; Inaba, H.; Matsuyama, M.; Lan, N. G.; Dokiya, M.; Tagawa, H. Structural Consideration on the Ionic Conductivity of Perovskite-Type Oxides. *Solid State Ionics* **1999**, *122*, 1−15.

(11) Kalinin, S. V.; Spaldin, N. A. Functional Ion Defects in Transition Metal Oxides. *Science* **2013**, *341*, 858−859.

(12) Cava, R. J.; Batlogg, B.; Chen, C. H.; Rietman, E. A.; Zahurak, S. M.; Werder, D. Single-Phase 60K Bulk Superconductor in Annealed $Ba_2YCu_3O_{7-\delta}$(0.3-less-than-δ-less-than-0.4) with Correlated Vacancies in the Cu-O Chains. *Phys. Rev. B: Condens. Matter Mater. Phys.* **1987**, *36*, 5719−5722.

(13) Bauer, U.; Yao, L.; Tan, A. J.; Agrawal, P.; Emori, S.; Tuller, H. L.; van Dijken, S.; Beach, G. S. D. Magneto-Ionic Control of Interfacial Magnetism. *Nat. Mater.* **2015**, *14*, 174−181.

(14) Bi, C.; Liu, Y.; Newhouse-Illige, T.; Xu, M.; Rosales, M.; Freeland, J. W.; Mryasov, O.; Zhang, S.; te Velthuis, S. G. E.; Wang, W. G. Reversible Control of Co Magnetism by Voltage-Induced Oxidation. *Phys. Rev. Lett.* **2014**, *113*, 267202. DOI: 10.1103/PhysRevLett.113.267202

(15) Jeen, H.; Choi, W. S.; Freeland, J. W.; Ohta, H.; Jung, C. U.; Lee, H. N. Topotactic Phase Transformation of the Brownmillerite $SrCoO_{2.5}$ to the Perovskite $SrCoO_{3-\delta}$. *Adv. Mater.* **2013**, *25*, 3651−3656.

(16) Khare, A.; Shin, D.; Yoo, T. S.; Kim, M.; Kang, T. D.; Lee, J.; Roh, S.; Jung, I.-H.; Hwang, J.; Kim, S. W.; Noh, T. W.; Ohta, H.; Choi, W. S. Topotactic Metal-Insulator Transition in Epitaxial SrFeOx Thin Films. *Adv. Mater.* **2017**, *29*, 1606, 1606566.

(17) Jeong, J.; Aetukuri, N.; Graf, T.; Schladt, T. D.; Samant, M. G.; Parkin, S. S. P. Suppression of Metal-Insulator Transition in VO_2 by Electric Field-Induced Oxygen Vacancy Formation. *Science* **2013**, *339*, 1402−1405.

(18) Kalabukhov, A.; Gunnarsson, R.; Borjesson, J.; Olsson, E.; Claeson, T.; Winkler, D. Effect of Oxygen Vacancies in the $SrTiO_3$ Substrate on the Electrical Properties of the $LaAlO_3/SrTiO_3$ Interface. *Phys. Rev. B: Condens. Matter Mater. Phys.* **2007**, *75*, 121404. DOI: 10.1103/PhysRevB.75.121404

(19) Liu, Z. Q.; Li, C. J.; Lu, W. M.; Huang, X. H.; Huang, Z.; Zeng, S. W.; Qiu, X. P.; Huang, L. S.; Annadi, A.; Chen, J. S.; Coey, J. M. D.; Venkatesan, T.; Ariando Origin of the Two-Dimensional Electron Gas at $LaAlO_3/SrTiO_3$ Interfaces: The Role of Oxygen Vacancies and Electronic Reconstruction. *Phys. Rev. X* **2013**, *3*, 021010. DOI: 10.1103/PhysRevX.3.021010

(20) Fuchs, D.; Pinta, C.; Schwarz, T.; Schweiss, P.; Nagel, P.; Schuppler, S.; Schneider, R.; Merz, M.; Roth, G.; von Loehneysen, H. Ferromagnetic order in epitaxially strained $LaCoO_3$ thin films. *Phys. Rev. B: Condens. Matter Mater. Phys.* **2007**, *75*, 144402. DOI: 10.1103/PhysRevB.75.144402

(21) Biskup, N.; Salafranca, J.; Mehta, V.; Oxley, M. P.; Suzuki, Y.; Pennycook, S. J.; Pantelides, S. T.; Varela, M. Insulating Ferromagnetic $LaCoO_{3-\delta}$ Films: A Phase Induced by Ordering of Oxygen Vacancies. *Phys. Rev. Lett.* **2014**, *112*, 087202. DOI: 10.1103/PhysRevLett.112.087202

(22) Jang, J. H.; Kim, Y.-M.; He, Q.; Mishra, R.; Qiao, L.; Biegalski, M. D.; Lupini, A. R.; Pantelides, S. T.; Pennycook, S. J.; Kalinin, S. V.; Borisevich, A. Y. *In Situ* Observation of Oxygen Vacancy Dynamics and Ordering in the Epitaxial $LaCoO_3$ System. *ACS Nano* **2017**, *11*, 6942−6949.

(23) Meng, D.; Guo, H.; Cui, Z.; Ma, C.; Zhao, J.; Lu, J.; Xu, H.; Wang, Z.; Hu, X.; Fu, Z.; Peng, R.; Guo, J.; Zhai, X.; Brown, G. J.; Knize, R.; Lu, Y. Strain-Induced High-Temperature Perovskite Ferromagnetic Insulator. *Proc. Natl. Acad. Sci. U. S. A.* **2018**, *115*, 2873−2877.

(24) Becher, C.; Maurel, L.; Aschauer, U.; Lilienblum, M.; Magen, C.; Meier, D.; Langenberg, E.; Trassin, M.; Blasco, J.; Krug, I. P.; Algarabel, P. A.; Spaldin, N. A.; Pardo, J. A.; Fiebig, M. Strain-Induced Coupling of Electrical Polarization and Structural Defects in $SrMnO_3$ Films. *Nat. Nanotechnol.* **2015**, *10*, 661−665.

(25) Hirai, K.; Kan, D.; Ichikawa, N.; Mibu, K.; Yoda, Y.; Andreeva, M.; Shimakawa, Y. Strain-Induced Significant Increase in Metal-Insulator Transition Temperature in Oxygen-Deficient Fe Oxide Epitaxial Thin Films. *Sci. Rep.* **2015**, *5*, 7894. DOI: 10.1038/srep07894

(26) Das, S.; Wang, B.; Cao, Y.; Cho, M. R.; Shin, Y. J.; Yang, S. M.; Wang, L.; Kim, M.; Kalinin, S. V.; Chen, L.-Q.; Noh, T. W. Controlled Manipulation of Oxygen Vacancies Using Nanoscale Flexoelectricity. *Nat. Commun.* **2017**, *8*, 156. DOI: 10.1038/s41467-017-00710-5

(27) Sharma, P.; Ryu, S.; Burton, J. D.; Paudel, T. R.; Bark, C. W.; Huang, Z.; Ariando; Tsymbal, E. Y.; Catalan, G.; Eom, C. B.; Gruverman, A. Mechanical Tuning of $LaAlO_3/SrTiO_3$ Interface Conductivity. *Nano Lett.* **2015**, *15*, 3547−3551.

(28) Yao, L.; Inkinen, S.; van Dijken, S. Direct Observation of Oxygen Vacancy-Driven Structural and Resistive Phase Transitions in $La_{2/3}Sr_{1/3}MnO_3$. *Nat. Commun.* **2017**, *8*, 14544. DOI: 10.1038/ncomms14544

(29) Zhang, Q.; He, X.; Shi, J.; Lu, N.; Li, H.; Yu, Q.; Zhang, Z.; Chen, L.-Q.; Morris, B.; Xu, Q.; Yu, P.; Gu, L.; Jin, K.; Nan, C.-W. Atomic-Resolution Imaging of Electrically Induced Oxygen Vacancy Migration and Phase Transformation in $SrCoO_{2.5-\delta}$. *Nat. Commun.* **2017**, *8*, 104. DOI: 10.1038/s41467-017-00121-6

(30) Gao, P.; Kang, Z.; Fu, W.; Wang, W.; Bai, X.; Wang, E. Electrically Driven Redox Process in Cerium Oxides. *J. Am. Chem. Soc.* **2010**, *132*, 4197−4201.

(31) Nellist, P. D., The principles of STEM imaging. In *Scanning Transmission Electron Microscopy*; Springer: 2011; pp 91−115.

(32) Kim, Y.-M.; He, J.; Biegalski, M. D.; Ambaye, H.; Lauter, V.; Christen, H. M.; Pantelides, S. T.; Pennycook, S. J.; Kalinin, S. V.; Borisevich, A. Y. Probing Oxygen Vacancy Concentration and Homogeneity in Solid-Oxide Fuel-Cell Cathode Materials on the Subunit-Cell Level. *Nat. Mater.* **2012**, *11*, 888−894.

(33) Abbate, M.; Fuggle, J. C.; Fujimori, A.; Tjeng, L. H.; Chen, C. T.; Potze, R.; Sawatzky, G. A.; Eisaki, H.; Uchida, S. Electronic Structure and Spin-State Transition of $LaCoO_3$. *Phys. Rev. B: Condens. Matter Mater. Phys.* **1993**, *47*, 16124−16130.

(34) Degroot, F. M. F.; Grioni, M.; Fuggle, J. C.; Ghijsen, J.; Sawatzky, G. A.; Petersen, H. Oxygen 1s X-Ray-Absorption Edges of Transition-Metal Oxides. *Phys. Rev. B: Condens. Matter Mater. Phys.* **1989**, *40*, 5715−5723.

DOI: 10.1021/acsami.9b08406
ACS Appl. Mater. Interfaces 2019, 11, 36800−36806

(35) Klie, R. F.; Ito, Y.; Stemmer, S.; Browning, N. S. Observation of Oxygen Vacancy Ordering and Segregation in Perovskite Oxides. *Ultramicroscopy* **2001**, *86*, 289−302.
(36) Wang, Z. L.; Yin, J. S.; Jiang, Y. D. EELS Analysis of Cation Valence States and Oxygen Vacancies in Magnetic Oxides. *Micron* **2000**, *31*, 571−580.

DOI: 10.1021/acsami.9b08406
ACS Appl. Mater. Interfaces 2019, 11, 36800−36806